Solution Properties of Glycogen. 1. Dilute Solutions

Catalina E. Ioan,† Thomas Aberle, and Walther Burchard*

Institute of Macromolecular Chemistry, University of Freiburg, 79104 Freiburg, Germany

Received April 20, 1999; Revised Manuscript Received August 16, 1999

ABSTRACT: Dilute solutions of glycogen from mussels (shellfish) and of different degradation steps were investigated by static and dynamic light scattering, viscometry, and end group analysis of the reducing end. The data were analyzed in comparison with theory for hyperbranched polymers. In the monomer of the $A\langle^{B_1}_{B_2}$ type, the functional group B_2 (resulting in α(1, 6) linkages) has a much lower reactivity than that of the B_1 group (leading to α(1, 4) linkages and chain growth). Qualitative agreement in behavior was found with the nonfractionated samples, but the effective branching density, derived from the applied physical techniques, was found to be considerably lower than that known from chemical analysis. SEC fractionation in on-line combination with multiple-angle laser light scattering and a viscosity detector revealed molar mass distributions that are composed of two main components. These components differ in their physical properties. The required examination was possible because R_g and $[\eta]$ could be measured for each slice. Shrinking factors $g = {R_g}^2_b/{R_g}^2_{lin}$ and $g' = [\eta]_b/[\eta]_{lin}$ were determined. The results of quantitative analysis are discussed in relation to current theories.

1. Introduction

Glycogen is an energy storage polysaccharide for most animals and is accumulated extracellularly. The molar mass varies in various species and can range from about 1.6×10^6 in the case of muscle glycogen up to about 300×10^6 for liver glycogen of mammals.[1−3] The latter displays a rosettelike, highly aggregated structure, as was recognized by electron microscopy.[4,5] For mammals, these aggregated structures are stored in the liver. In the present study, a glycogen from mussels was chosen. It differs from the former by not being stored in the liver, and it does not occur in an organized aggregated form. Its molar mass varies for different shellfish species and has values between 1.5×10^6 and 8×10^6. In the present case, the molar mass was $M_w = (8.12 \pm 0.2) \times 10^6$. The repeating unit of glycogen is the α(1, 4) linked glucose which contains about 8% of additional α(1, 6) glycoside bonds;[6] i.e., 8% of the monomer units in the polymer are branching units. Glycogen has essentially the same chemical structure as amylopectin, which is the branched component in starches. Amylopectin, however, is much larger ($M_w \cong (75 \pm 20) \times 10^6$)[7] and considerably less branched, having only 4−5% branching units.

The material of our study is of interest for two main reasons. First, glycogen is a biopolymer. A high branching density is an efficient measure to keep the energy stored in a rather compact, space-saving structure. On the other hand, the enzymes should have access to internal parts of the polysaccharide to guarantee a quick degradation when glucose is needed as energy source. For a better understanding of this mechanism, it is essential to know details of its structure. Second, the study of this type of branched structure has become a topic of principal interest in recent activities of polymer research. Glycogen and amylopectin appear to be a biological realization of so-called hyperbranched polymers. These are polymers which are built up of $A\langle^{B_1}_{B_2}$ monomers in which the different functionalities A, B_1, and B_2 can react only under a strict constraint: bonds are possible only between A and B_1 or A and B_2. This constraint can lead to a high branching density, but in contrast to the statistical polymerization of trifunctional monomers, no permanent gel can be formed.[8−10] At present, much effort is being invested by organic chemists to realize these structures, first predicted by Flory.[8] These attempts have not been very successful in preparing high-molar-mass polymers because of side reactions, among which ring formation is presumably most disturbing because ring formation would stop further growth.

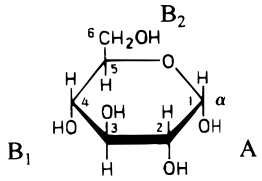

α-D-glucose

Figure 1. Monomer unit in glycogen. The reducing end group in C1 (A) forms the focal functionality in a hyperbranched molecule of the $A\langle^{B_1}_{B_2}$ type, where B_1 and B_2 are the nonreducing OH-groups used by enzymes in the formation of glycogen. For further details, see text.

The hyperbranched structure of glycogen and amylopectin becomes clear during examination of the structure of its repeating unit, glucose (Figure 1). Glucose has one reducing end group in C_1, which in the model furnishes the functional group A (now often denoted as focal functionality). Furthermore, there are four nonreducing OH end groups in C_2, C_3, C_4, and C_6. Because of the specificity of enzymes, only reaction between C_1 and C_4 (chain growth) and C_1 and C_6 (branching) are possible in glycogen and amylopectin. Apparently, because of this specificity, ring formation is suppressed and leads to the aforementioned surprisingly high molar masses. Thus, these biopolymers seem to be ideal models for the study of hyperbranching.

Our report will be divided in several parts to be published in separate papers. In the present contribu-

† Permanent address: "P. Poni" Institute of Macromolecular Chemistry, 6600 Iasi, Romania.

10.1021/ma990600m CCC: $18.00
Published on Web 10/02/1999

tion, the properties at high dilution are studied using static and dynamic light scattering and viscometry. Further details are drawn from size exclusion chromatography (SEC) in on-line combination with multiple-angle laser light scattering (MALLS) and a viscosity detector. In contrast to the former techniques (where measurements were done with unfractionated samples), the latter gives valuable information on the structure of narrowly distributed fractions. The proper treatment of data supplied by SEC with such detector combinations, and the interpretation of the results is rather involved and will be outlined in a consecutive paper.

In a third paper, we consider fairly concentrated solutions. The behavior of *linear chains* in semidilute solution is now well-established,[11] but little has been done so far with *branched* macromolecules.[12,13] As was outlined in previous papers elsewhere[14,15] new effects are to be expected because a complete interpenetration of segments from different macromolecules no longer is possible because of the obstacles generated by the branching units. Because glycogen is stored in the tissue in clusters, the study of highly concentrated solutions is also of biological interest.

2. Theoretical Background

In the course of his studies on the formation of branched structures with macromolecules, Flory[8] discovered that very high branching densities can be obtained with AB_f monomers without passing a gel point. Gelation is principally prevented if only A-functionalities can form a bond with B-functionalities and all other reactions are excluded. The incapability of network formation becomes clear when the extents of reactions α and β for the functional groups A and B are introduced. The extent of reaction α, for instance, is the fraction of all functional A groups in the system that have formed a bond. Because of the stringent constraint that only A−B bonds are possible one has

$$\alpha = f\beta \tag{1}$$

where f is the number of B-functional groups in a monomer. As in random f-functional polycondensation, branched clusters are formed which grow in size with increasing α. Infinitely large clusters, however, are reached only at $\alpha = 1$ or complete monomer conversion.

Flory derived equations for the number- and weight-average molar mass and the corresponding polydispersity as follows:

$$M_n = M_0/(1 - \alpha) \tag{2}$$

$$M_w = M_0\frac{1 - \alpha^2/f}{(1 - \alpha)^2} \tag{3}$$

$$\frac{M_w}{M_n} = \frac{1 - \alpha^2/f}{1 - \alpha} \qquad \alpha \to 1: \frac{f-1}{f}\,DP_n \cong \left(\frac{f-1}{f}\,DP_w\right)^{1/2} \tag{4}$$

where the arrow indicate the limit of high degrees of polymerization. In contrast, for random branching, one has $M_w/M_n \approx DP_w$, whereas in A−B_f branching, $M_w/M_n \approx DP_w^{1/2}$. A much narrower distribution than for the A_f polymerization is obtained. Flory-type branching with f equal reactive B groups was soon extended by Erlander and French[9] to monomers in which all B groups differ in their reactivity. The $A\langle^{B_1}_{B_2}$ type (or $A\langle^{B}_{C}$) of monomer is in the present paper of special interest. Now, the chemical constraint leads to

$$\alpha = \beta_1 + \beta_2 \tag{5}$$

It is convenient to introduce an additional parameter p by writing

$$\beta_1 = \alpha(1 - p) \qquad \beta_2 = \alpha p \tag{6}$$

Let B_2 be the functional group that is less reactive than B_1. Depending on the values of $p \leq 1$, one has three limiting cases: (i) for $p = 0$, only a linear chain growth is possible via (AB_1)-bonds; (ii) for $p = 1$, again, linear chain growth occurs, but now via AB_2-bonds; and (iii) equal reactivity for both functionalities is obtained when $p = 0.5$. The fraction $(1 - p)$ in eq 6 denotes the probability that an A−B_1 bond was formed, and p is the probability that an A−B_2 bond instead of an A−B_1 bond was formed. Often $p \ll 1$ and $(1 - p)$ can then be considered as a chain-growing probability with a length distribution of

$$h(x,p) = (1 - p)^{x-1}p$$

indicating the frequency that after $x - 1$ successive A−B_1 bonds a link is introduced via an A−B_2 bond. Thus, p is not yet the probability for branching. Branching occurs when both B_1 and B_2 have reacted, which gives

$$p_B = (1 - p)p \tag{7}$$

Among others, this definition allows the calculation of the number of branching units in a macromolecule. Because $\alpha^2 p(1 - p)$ is the probability that a monomer unit selected at random is a branching unit, one simply solves for the number of branching units per number- and weight-average degree of polymerization

$$B_n = \alpha^2 p(1 - p)DP_n \tag{8}$$

$$B_w = \alpha^2 p(1 - p)DP_w \tag{9}$$

The branching density is usually defined as the ratio of branching units n_b in the system to all monomers N built in a polymer: $B/N \equiv n_b/N$. This ratio is very close to the ratio of number averages in B_n/DP_n. Thus, the branching probability $p_B = p(1 - p)$ and the branching density B/N become identical for large DP_n, where $\alpha \cong 1$. Differences, however, become noticeable for $\alpha < 1$, i.e., in the oligomeric region of hyperbranching process. For another definition of the branching density, see Appendix 1.

3. Experimental Section

Samples. Glycogen from mussel (type VII) was a product of Sigma. To obtain fractions of different molar masses, a controlled degradation by acid hydrolysis was carried out. The glycogen was suspended in methanol, and different amounts of concentrated HCl were added at room temperature (4 g of glycogen + 20 mL of MeOH + x ml of HCl) (see Table 1). Each mixture was shaken for 4 days, at which time, according to literature,[16] the limiting value is reached. The degraded samples were neutralized with 1 M NaOH and washed with methanol.

Dry Substance Content. This value was determined in a moisture analyzer (Sartorius MA 40). The obtained values were around 87%.

Table 1. Characteristic Parameters of Starch Fractions Obtained by Acid Hydrolysis in Methanol Suspensions (4 g Glycogen + 20 mL Methanol + *x* mL HCl)

			SLS ($\lambda = 488$ nm) in NaOH					SLS ($\lambda = 632.8$ nm) in water					
sample	HCl (ml)	DS (%)	$M_w \times 10^{-6}$ (g/mol)	$A_2 \times 10^6$ (mol ml/g^2)	R_g (nm)	R_h (nm)	$[\eta]$ (ml/g)	$M_w \times 10^{-6}$ (g/mol)	$A_2 \times 10^6$ (ml mol/g^2)	R_g (nm)	R_h (nm)	$[\eta]$ (ml/g)	$M_n \times 10^{-5}$ [a] (g/mol)
G		86	8.120	3.92	25	25	6.90	6.600	1.84	28	28	6.67	27.140
G1	0.3	90	5.240	4.38	21	21		4.720	3.89	18	21	6.37	
G2	0.6	86	2.900	7.03	22	20		2.580	3.90			7.87	3.005
G3	1.0	87	2.880	7.11	20	19	6.96	1.919	7.39	12	16	6.63	
G4	1.4	83	2.380	8.24	21	15	7.71	1.420	8.77	15	17	7.24	1.280
G5	2.0	88	1.590	16.60	18	16		0.960	18.70	10	13	7.44	
G6	3.0	88	0.945	20.10	10	13	7.67	0.783	25.10				0.437
G7	3.6	86	0.769	18.60	9	14	7.45						
G8	4.0	88	0.761	17.50	12	14		0.523	20.10	10	12	7.24	
G9	5.0	83	0.326	54.00	16	11	8.04	0.235	78.60				0.673

[a] Method of Nelson−Somogyi.

Number-Average Molecular Mass. M_n was obtained by the reducing end group determination. Following the method of Nelson−Somogyi,[17] M_n was obtained as follows. Three different solutions were prepared. Solution 1: 25 g of Na_2CO_3, 25 g of K−Na−tartrate·4 H_2O, 20 g of $NaHCO_3$, and 200 g of Na_2SO_4 dissolved in 1 L of water. Solution 2: 15 g of $CuSO_4$·5 H_2O and 2 drops of concentrated H_2SO_4 in 100 mL of water. Solution 3: (a) 25 g of $(NH_4)_6Mo_7O_{24}$·4 H_2O and 21 mL of concentrated H_2SO_4 in 450 mL of water; (b) 3 g of Na_2HAsO_4·7 H_2O in 25 mL of water. Solutions 3a and 3b were mixed and stored in a brown vessel. The copper reagent was freshly prepared before using, by adding 1 mL of solution 2 to 25 mL of solution 1. Copper reagent (1 mL) was added to 1 mL of the glycogen solution in a 10 mL vessel and kept 20 min in a boiling water bath. Red Cu(I) was precipitated. The solution then was cooled to room temperature in a cold water bath. After 5 min, 1 mL of solution 3 was added, and the mixture was shaken. Cu(I) was dissolved in a deep blue complex. After a further 5 min, the vessel was filled with distilled water to 10 mL. After 5 more minutes, the extinction was measured at $\lambda = 540$ nm. To establish the calibration curve, maltotriose solutions of different concentrations were used.

Static Light Scattering (SLS). SLS measurements were performed with fully computerized and modified SOFICA photogoniometers (G. Baur, Instrumentenbau, Hausen, Germany). The one was equipped with a He−Ne laser ($\lambda_0 = 632.8$ nm) and the other with an Ar-ion laser ($\lambda_0 = 488$ nm). Measurements were made in an angular region from 35 to 145°, in steps of 5°, at 20 °C. Two different solvents were used: water ($dn/dc = 0.151$ mL/g) and 0.5 N NaOH ($dn/dc = 0.142$ mL/g), where dn/dc denotes the refractive index increment that was determined with a Brice-Phoenix differential refractometer. The concentrations in all cases were between 0.2 and 2%.

Dynamic Light Scattering (DLS). DLS measurements were carried out using an ALV photogoniometer (ALV, Langen, Germany) equipped with an ALV 5000 correlator. Measurements were made in an angular range from 30 to 150°, now however, in steps of 10°, at 20 °C.

Size Exclusion Chromatography. Analytical fractionation of the samples was carried out by SEC in on-line combination with an MALLS instrument (DAWN, Wyatt Technology, Santa Barbara) and with a RI/VISC detector (Knauer, Berlin, Germany) that allowed the detection of concentration and viscosity. The chromatography was driven by an HPLC pump 64 (Knauer, Berlin, Germany) at a pressure of 10 bar. The injection volume was 50 μl. As elution solvent, a 0.1 M $NaNO_3$ solution containing 0.05% NaN_3 was chosen. The addition of sodium acid was necessary to prevent bacterial growth. A 20 μm Suprema 10 000 column from Polymer Standards Service (Mainz, Germany) was employed.

Viscosity. Measurements were made with an automatic Ubbelohde viscometer (Schott, Germany) at 20 °C in water and in 0.5 N NaOH. A capillary of 0.63 mm in diameter was used.

4. Results

Properties of Nonfractionated Samples. Nine samples of different molar masses were prepared by acid hydrolysis of glycogen in methanol suspensions, as described in the Experimental Section (Table 1). The samples were measured at 20 °C by static light scattering from concentrations of 0.2−2%. The angular range was 35−145°, and the scattering intensity was registered in steps of 5° Measurements were made with blue light ($\lambda_0 = 488$ nm) for the samples dissolved in 0.5 N NaOH. For a better comparison with SEC results, we also performed light scattering measurements in pure water using red light ($\lambda_0 = 632.8$ nm) of the same wavelength as that in the DAWN instrument for MALLS.

*Static and Dynamic Light Scattering***.** Figure 2 shows a Berry plot from the parental glycogen (nondegraded). The Berry plot differs from the more familiar Zimm plot by the fact that the *root* of Kc/R_θ is now plotted. From the intercept, the weight-average molar mass M_w is obtained. From the slope of the angular dependence, the radius of gyration R_g is found, and from the concentration dependence, the second virial coefficient A_2 is derived. The Berry plot has, among others, the advantage that it also takes into account the influence of the third virial coefficient.

The molar mass M_w dependence from the radius of gyration R_g is shown in Figure 3. Compared to the high-molar-mass M_w, the radius of gyration R_g is small, but this is a consequence of high branching density. These data are compared with the hydrodynamic radii R_h measured with the same solution by dynamic LS. A fairly well-defined straight line can be drawn through the R_h points. In dynamic light scattering, radii down to about 3 nm can be measured with high accuracy. However, the limit for R_g in static light scattering lies at about 10 nm. The scatter of data becomes very large, and the value for the lowest molar mass M_w is no longer reliable. The observed high value probably results from traces of dust.

For a first estimation of the polymer structure, it is instructive to form the ratio $R_g/R_h \equiv \rho$. Within experimental error, there is no change in the molar mass, which could be expected because both radii should have the same molecular weight dependencies. In Figure 3, the molar mass M_w dependence of the radius of gyration R_g for linear amylose is also plotted.[35b] This relationship will be needed later for the determination of the shrinking factor g.

Finally, in Figure 4, the molar mass dependence on the second virial coefficient A_2 is shown and compared with the relationship for linear amylose. The points of measurement follow a power law $A_2 = KM^{a_{A_2}}$ with an exponent of $a_{A_2} = -0.8$. The much larger negative

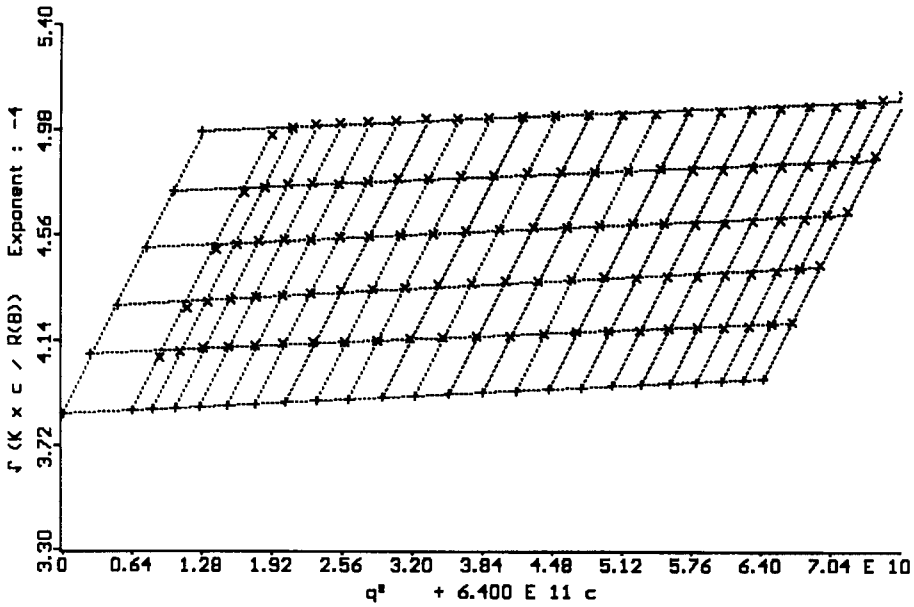

Figure 2. Berry plot from the nondegraded glycogen (from mussels) in 0.5 N NaOH: $M_w = 8.12 \times 10^6$, $R_g = 25$ nm, and $A_2 = 3.92 \times 10^6$ mol mL/g^2. The resulting overlap concentration is $c^* = 31.4$ g/L.

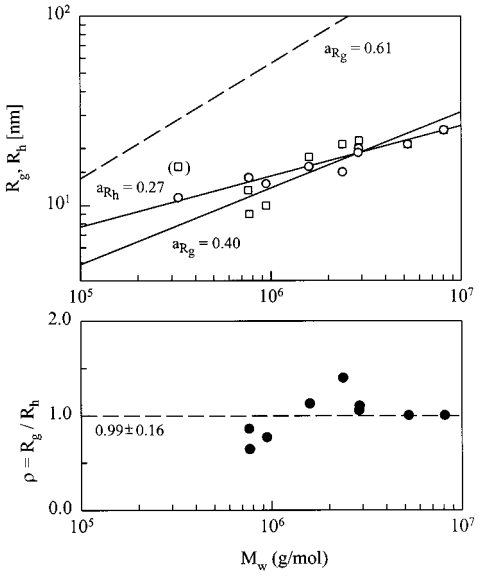

Figure 3. Molar mass dependencies of the radius of gyration (square symbols) and the hydrodynamic radius (circular symbols) for the original glycogen and nine degradation steps (upper part) and the ratio $\rho = R_g/R_h$ of the two radii as a function of the molar mass M_w. The dashed line in the upper part of the curve with an exponent of $a_{R_g} = 0.61$ refers to linear amylose in the same solvent.[35b] The ρ-parameter is involved with a fairly large error, and the dashed line corresponds to the average but needs not necessary mean independence of M_w.

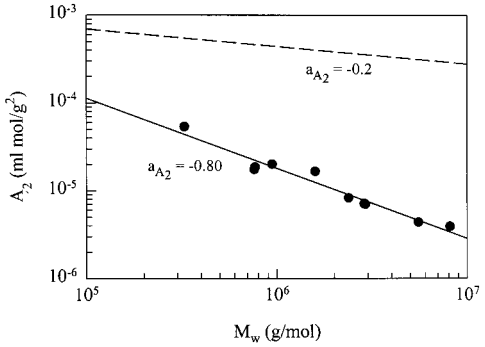

Figure 4. Molar mass dependency of the second virial coefficient A_2 from the nonfractionated glycogens (full line) compared to the corresponding dependency of amylose (dashed line). From the ratio of both curves, the shrinking factor $g_{A_2} = A_{2\ \text{branched}}/A_{2\ \text{linear}}$ can be calculated (see also Figure 11).

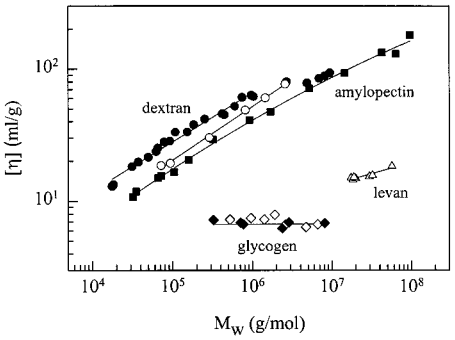

Figure 5. Molar mass dependency of the intrinsic viscosity [η] for several hyperbranched polysaccharides. Levan[36] is based on fructose, and the others are all based on α-glucose. Note the low viscosity of glycogen and the independence of molar mass. Filled symbols: in 0.5 N NaOH. Open symbols: in water.

exponent compared to that for amylose is characteristic of branched structures[18] (see Discussion).

Viscosity. Intrinsic viscosities [η] were measured in an Ubbelohde viscometer. Very low values for [η] were found, which show no molar mass dependence. The results are plotted in Figure 5, together with the data from other branched polysaccharides. Dextran, amylopectin, and glycogen are composed of the same monomer unit, i.e., glucose. Levan differs slightly from dextran, because the monomer unit here is fructose. The decrease of the intrinsic viscosity is expected and is an indication for the increase in branching density. Accordingly, dextran has the lowest branching density, followed by amylopectin and levan. Apparently, glycogen has the highest branching density.

Polydispersity. Polydispersity was determined from measurements of the number-average M_n by end group analysis in combination with M_w from SLS. The data of M_w/M_n are plotted in Figure 6 against $M_w^{0.5}$. Within the scatter of data, approximately the same curve was

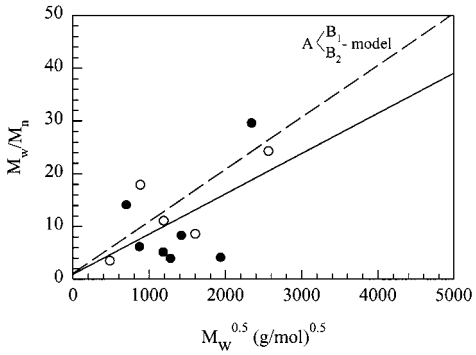

Figure 6. Polydispersity of glycogen as a function of the root of the molar mass M_w. Open symbols were determined from end group analysis, and the filled symbols are the results of SEC. The dashed line corresponds to the ideal hyperbranching process with $p \cong 0.008$. The full line represents the regression to all points.

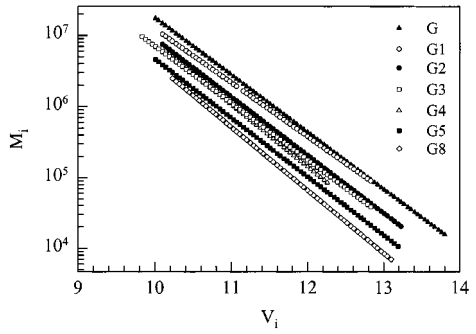

Figure 7. Dependence of the molar mass from the elution volume in SEC−MALLS for seven glycogens used in this study. Actually, these calibration curves are well-defined only in the range where both the light scattering and the RI signal are sufficiently large. Large scatter occurs at the edges of high and low molar masses. The present lines correspond to linear *extensions* into these regions.

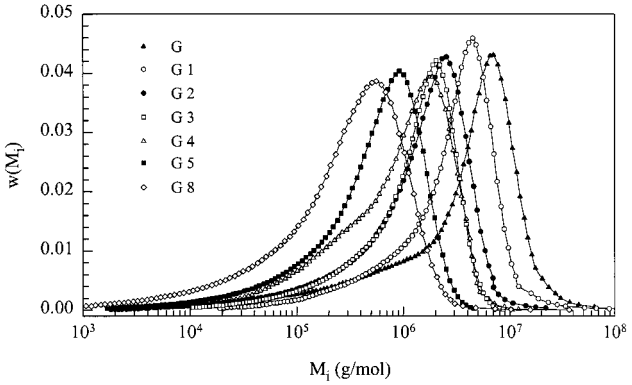

Figure 8. Molar mass distribution derived from SEC−MALLS with the calibration curves shown in Figure 7. Note that the calibration curves are systematically shifted to lower molar masses for the degraded glycogens.

obtained as from the SEC data. The increase qualitatively corresponds to expectation. However, see Discussion for details.

Properties of Narrow Fractions. *Molar Mass Distribution from SEC Combined On-Line with MALLS.* From seven samples, the weight fraction molar mass distributions $w(M_i)$ were determined. The calibration curves of the molar mass as a function of the elution volume is shown in Figure 7. The resulting molar mass distributions are plotted in Figure 8 in a logarithmic scale for the molar mass M_i. The weight fraction molar

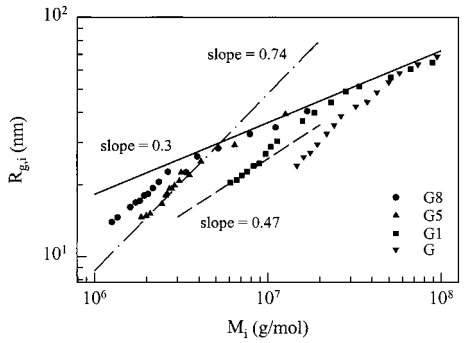

Figure 9. Molar mass dependence of the radius of gyration for four samples (G, G1, G5, G8) derived from SEC−MALLS. All curves show two different slopes. The high-molar-mass region of all samples follows the behavior of hard spheres with a slope of 0.3. For the other slopes, see the Discussion. A cut was made at low and high molar masses because of the large scatter of data as mentioned in Figure 7. For this reason, the average R_{gz} in Table 2 appears smaller than the result that could be expected from the curves. The calibration curves of Figure 7 were not needed.

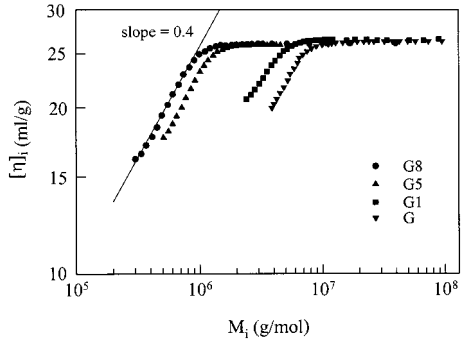

Figure 10. Intrinsic viscosity dependence on the molar mass for the same samples as in Figure 9. The results were obtained from SEC−MALLS in combination with a viscometer VISC. Again, as in Figure 9, all curves are composed of two sections. The independence of the intrinsic viscosity $[\eta]$ indicates hard sphere behavior. Applying the scaling relationship between ν and a_η ($a_\eta = 3\nu - 1$) gives a slope of 0.33, which is close to the line in Figure 9. A similar cut was made as described in Figure 9. Note that this is only a tentative explanation. For the deviation of this limiting slope, see discussion in the text.

mass $w(M_i)$ is derived from the cumulative distribution $W(M_i)$ as $w(M_i) \equiv dW(M_i)/dM_i$ (Note: this distribution has not to be confused with the more often used distribution $dW(M_i)/d \log M_i = w(M_i)M_i$). All samples show more or less the same shape.

With the on-line combination of MALLS and VISC it becomes possible to determine for each slice the radius of gyration and the intrinsic viscosity. The results are shown in Figures 9 and 10, respectively, for four selected samples. Both relationships show unusual behavior. Without any specific analysis, it is clear that the material structure is built of two components.

The averages of M_n, M_w, and M_z and $R_z \equiv (\langle R_g^2 \rangle_z)^{1/2}$ can be found in the usual manner from the individual data of the slices and are given in Table 2.

5. Discussion

Branched samples have characteristics of rather broad size distributions. Such broad distributions have incisive influence on the radii (R_g and R_h), the second virial coefficient A_2, and the intrinsic viscosity $[\eta]$.[13,19,20] Despite this overlap with structural parameters, it remains instructive to examine the molar mass depend-

Table 2. Average Molecular Weights and *z*-Average Radius of Gyration Obtained from SEC

sample	$M_n \times 10^{-5}$ (g/mol)	$M_w \times 10^{-6}$ (g/mol)	$M_z \times 10^{-6}$ (g/mol)	R_z (nm)
G	2.079	6.155	12.490	26
G1	9.098	3.754	7.007	24
G2	2.441	2.023	3.462	20
G3	4.170	1.630	2.487	17
G4	2.722	1.396	2.466	16
G5	1.230	0.758	1.276	15
G6				
G7				
G8	3.446	0.488	1.096	16
G9				

Table 3. Exponents in the Power Law $Y = k_y M_w^{a_y}$

			a_y calcd from	
Y	a_y	$a_{y\,exp}$	a_{A_2}	$a_{[\eta]}$
R_g	ν	0.40	0.40	0.33
R_h	ν	0.27	0.40	0.33
A_2	$a_{A_2} = 3\nu - 2$	−0.8		−1
$[\eta]$	$a_{A_2} = 3\nu - 1$	0	0.2	

Table 4. Parameters $\rho = R_g/R_h$ and Ensemble Fractal Dimensions for Various Macromolecular Architectures

architecture	solvent	ρ	$d_f = 1/\nu$
random coil, linear chain, and polydisperse	good	2.050	1.7
	Θ-condition	1.730	2.0
randomly branched chain	good	1.732	2.0
	poor	1.732	2.5
hyperbranched	Gaussian statistics	1.225	4.0
glycogen, experimental	good	0.994	2.8
hard sphere		0.778	3.0

encies of the radii, the second virial coefficient, and the intrinsic viscosity. For self-similar structures, *scaling relationships* exist between the exponents in the power law dependencies, which in general terms can be written as

$$y = K_y M_w^{a_y} \tag{10}$$

The results of the scaling check are collected in Table 3. Because the accuracy of the viscosity and the second virial coefficient data are most reliable, we applied the scaling laws from the second row in Table 3 to calculate the exponent ν. The results show fairly large deviations but are in the same range as those found for R_g and R_h. Within the scatter of data, the scaling laws are seemingly fulfilled. Under the assumption of self-similarity,[13] an ensemble fractal dimension of $1/\nu = d_{fe} = 2.86$ is derived. This value is considerably higher than that predicted for randomly branched materials in the reaction bath, i.e., 2.5. On the other hand, the samples do not adopt the fractal dimension of hard spheres with $d_{fe} = 3$. Table 4 presents a list of predicted ensemble fractal dimensions d_{fe} for different molecular architectures.[20] The apparent fractal dimension gives a first impression on the molecular architecture.

Another structure relevant parameter is obtained from the ratio $\rho = R_g/R_h$. For self-similar structures, there should be no molar mass dependence; the value of ρ is related to the segment density in the macromolecule.[21] Within the scatter of the data, this behavior is in fact observed and a value of $\rho = 0.99 \pm 0.16$ is obtained. Very similar results were obtained with degraded amylopectin.[22] The theoretically predicted asymptotic ρ-parameter for hyperbranched structures is $\rho = 1.22$, which is about 20% higher than that measured.[21] However, the theoretically predicted value is based on the Kirkwood approximation for the hydrodynamic interaction,[23,24] which according to simulations by Freire et al.[25] results in values that are about 23% larger. In fact, our value agrees with the simulated ρ value of 0.92 ± 0.01 obtained for a 12-arm star at large M_w. Thus, the observed ρ-parameter would be in good agreement with that of the hyperbranched structures. The value is not far away from the behavior of hard spheres. (see Table 3)

A third way of characterizing branched structures is via the *shrinking factors*.[18,22,26,27] These are defined as the ratio of the branched to the linear quantities at the same molar mass. Three parameters can be defined in this manner: g, g', and g_{A_2}.[18,22,27]

$$g = \frac{R_{g\,branched}^2}{R_{g\,linear}^2} \tag{11}$$

$$g' = \frac{[\eta]_{branched}}{[\eta]_{linear}} = \frac{\phi_{branched}}{\phi_{linear}} g^{3/2} \tag{12}$$

$$g_{A_2} = \frac{A_{2\,branched}}{A_{2\,linear}} = \frac{\psi_{branched}}{\psi_{linear}} g^{3/2} \tag{13}$$

In these equations, $\phi_{branched}$ and ϕ_{linear} denote the prefactors in the Fox−Flory equation for branched and linear chains. Similarly, the symbols $\psi_{branched}$ and ψ_{linear} denote the coil interpenetration functions (see Yamakawa[24]).

The molar mass dependence of these parameters is displayed in Figure 11. The shrinking factor g for randomly branched samples was calculated by Zimm and Stockmayer,[26] which for *narrow fractions* of three-functional monomers is given by the equation

$$g_j = \left[\left(1 + \frac{n_j}{7}\right)^{1/2} + \frac{4n_j}{9\pi}\right]^{-1/2} \tag{14}$$

where the n_j are the number of branching points in the macromolecule. Assuming constant branching density for the various samples, we can consider the proportionality between the molar mass and the number of branching points as

$$M_j = M_0 n_j \equiv \frac{1}{\lambda} n_j \tag{15}$$

where M_0 is the molecular weight of the branching unit and λ is introduced here for rewriting g_j in terms of M_j:

$$g_j = \left[\left(1 + \frac{\lambda M_j}{7}\right)^{1/2} + \frac{4\lambda M_j}{9\pi}\right]^{-1/2} \tag{14'}$$

Knowing M_0 for an A_3-monomer unit, the chain length between two branching points is than $l_b = {}^2/_3 M_0/162$. However, in the $A\begin{pmatrix}B_1\\B_2\end{pmatrix}$-monomer-type, one has two long chains in the B-positions but none in the A position. Thus, now the chain length between two branching units is $l_b = {}^1/_2 M_0/162$.

This results have to be distinguished from the hyperbranched model.

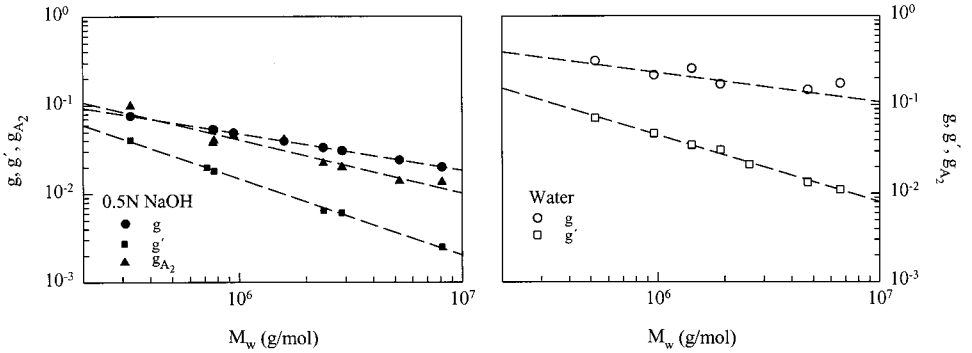

Figure 11. Shrinking factors of the nonfractionated samples as a function of M_w (see eqs 11−13) for glycogens in 0.5 N NaOH and in water.

For nonfractionated, hyperbranched samples, the g_{Hb}-factor was derived by one of the present authors and resulted in the relationship[29a,b]

$$g_{Hb} = \frac{6(1 + 2B_w)^{1/2}}{[1 + (1 + 2B_w)^{1/2}]^2} \tag{16}$$

with $B_w = p(1 - p)DP_w$, which is the number of branching points based on the weight-average degree of polymerization or

$$g_{Hb} = \frac{6(1 + 2qM_w)^{1/2}}{[1 + (1 + 2qM_w)^{1/2}]^2} \tag{16′}$$

where $q = p(1 - p)/M_0$. In the strict theory, $M_0 = 162$ is not a fit parameter. However, this value can also be considered as a fit parameter, and a deviation from $M_0 = 162$ then would give indications for a more complex structure. This relationship for g differs only slightly from that in eq 14, when n_j is replaced by B_w. Both represent the number of branching units in a macromolecule. However, the Zimm−Stockmayer relationship (14) refers to monodisperse fractions derived from a *random* branching process, whereas eq 16 is related to nonfractionated samples in which the branching process was restricted by a stringent constraint.

A quantitative description of the g'-factor in terms of the branching density has not yet been fully successful. Uncertainties arise from the hydrodynamic interactions among the segments in a polymer. The treatment of the many-body problem embodies mathematical difficulties that so far could not exactly be solved. The relationship of eqs 12 and 13 suggest, however, a unique relationship between g' and g and a similar one for g_{A_2} and g. Tentatively, a power law interdependence has been assumed[18,28,30]

$$g' = g^{b_\eta} \tag{17}$$

$$g_{A_2} = g^{b_{A_2}} \tag{18}$$

Polydisperse, Nonfractionated Samples. When eq 14′ is applied, the proportionality factor will be the molar mass of a repeating unit that consists of two short chains connected to the two B-functionalities. A fit of the experimental curves in Figure 11 with eq 14′ would give $M_0 = 706$, which corresponds to a chain segment of about 2.2 glucose units between two branching points, including 1 branching unit. However, this fit is incorrectly made for polydisperse samples with a theory for *monodisperse* fractions. Applying, on the other hand, eq 16′, one finds $M_0 = 128$, which is smaller than even one glucose unit with $M_{glucose} = 162$. In other words, no physically sensible fit is found.

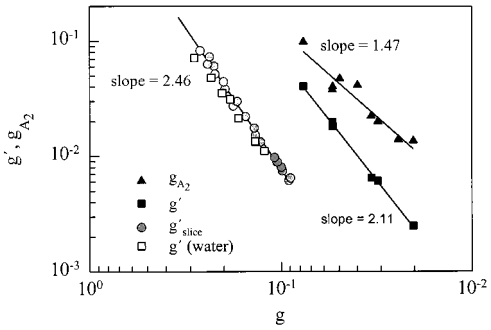

Figure 12. Shrinking factors g' and g_{A_2} versus g for the nonfractionated and fractionated samples. Note that when g'_{slice} is used these values were plotted against g_{slice}, whereas in all other cases, g refers to the nonfractionated samples.

Figure 12 exhibits the double logarithmic plot of g' and g_{A_2} against g. The slopes gave exponents of $b_\eta = 2.46$ (for measurements in water), $b_\eta = 2.11$, and $b_{A_2} = 1.47$ (for measurements in 0.5 N NaOH). The b_η exponent deviates considerably from those found for fractions of randomly branched three-arm polysterene macromolecules with $b_\eta \cong 0.6$[28] and from the theoretically predicted limiting values, i.e., 0.5 (Zimm and Kilb[31]) and 1.5 (Stockmayer and Fixman[27]). As was already mentioned, this anomaly may have its basis in a certain branching heterogeneity. Furthermore, the molar mass distribution is much more narrow than that predicted by a statistical theory.

The failure in finding a meaningful fit for the branching density with the shrinking factors gives indications for a branching process that is more biosynthetically complex than that derived from the idealized theory, which is based on a statistical process.

Properties of Slices. To get further insight in the mechanism, we performed SEC in on-line combination with light scattering (MALLS) and viscosity (VISC). The experimental setup has the advantage that the molar mass in each slice is directly measured as a function of the elution volume. For linear and self-similar macromolecular structures, this calibration curve agrees within experimental error with those of various samples of different M_w. In the present case, however, the calibration curve is shifted to lower molar masses M_i when the parental sample is progressively degraded. This behavior requires a special discussion which will be postponed to a separate paper. Unexpectedly, the various samples form no common curves when R_{gj} or

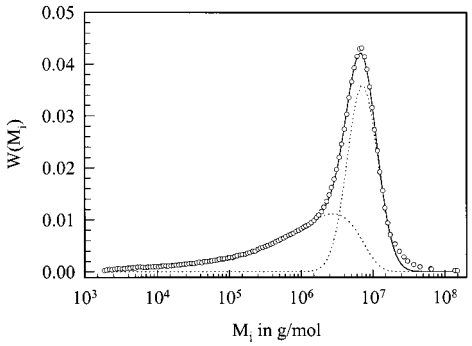

Figure 13. Molar mass distribution of the original nondegraded glycogen. The distribution is clearly composed of two components. Analysis was made by Peak Fit (Jandel Scientific).

$[\eta]_j$, respectively, are plotted against M_j. Clearly, no self-similarity is obtained. A hint for such behavior may be taken from Figure 8. It shows the corresponding molar mass distributions. Evidently, the distribution is composed of two components as may be recognized more clearly from Figure 13. The effect of these two components also becomes visible when the molar mass dependence of the radius of gyration (Figure 9) and the intrinsic viscosity (Figure 10) are considered. Clearly, the lower mass component in the distribution shows behavior different from that of the high-molar-mass component.

Striking is the independence of the *intrinsic viscosity* when a certain molar mass is exceeded. Such behavior is predicted for spheres with homogeneous segment density, which according to Einstein

$$[\eta] = \frac{2.5}{d_{\text{segment}}} \tag{19}$$

gives $d = 0.096$ g/mL. This value corresponds to the internal concentration in a homogeneous sphere. The particle are still highly swollen. Assuming the scaling relationship for the radius of gyration, one would get an exponent of 0.33, representing the slope in the plot of R_g against M_w (Figure 9). This predicted exponent agrees very well with the line that can be drawn through the points of the high-molecular-weight slices. This gives evidence for hard sphere behavior of the high-molar-mass component in the distribution. For the lower mass component in the distribution, we find a clear molar mass dependence for the viscosity and a much higher exponent of the radius of gyration. These two slopes for the viscosity and the radius of gyration no longer show scaling behavior, because with an exponent of $a_\eta = 0.4$ one should obtain an exponent of $\nu = 0.47$; however, a value of 0.74 is obtained. The predicted slope is approximately obtained for the lowest molar masses. This leads to a tentative explanation that the high exponent of 0.74 may be the result of an overlap of the two components in the distribution. This effect will be more pronounced for the radius of gyration, in which, because of the *z*-average, the high molar masses from a mixture of two components is more strongly weighed than is the case for the intrinsic viscosity.

Because from each slice in SEC the molar mass, radius of gyration, and intrinsic viscosity simultaneously were measured and the corresponding data for uniform synthetic amyloses (the linear counterparts) are known,[35] *the shrinking factors* g and g' now could be determined for *monodisperse fractions*. Figure 12 shows the result in a plot of g' as a function of g, and the data are compared with the corresponding data from the nonfractionated samples. In addition, g_{A_2} versus g is also shown. Two noticeable observations can be stated. First, the curves for the nonfractionated samples appear to be shifted to smaller g values by approximately a factor of 3, but the slopes in the double-logarithmic scale are not significantly altered. Second, the solvent quality has almost no influence on the curve; the data from the aqueous solution form a curve with the same slope and are only slightly shifted to larger g. The slopes of 2.11 and 2.46, respectively, are much larger than 1.5 and cannot be explained so far, with any existing theory. Here, it has to be emphasized that only those fractions were used that display no molar mass dependence of intrinsic viscosity.

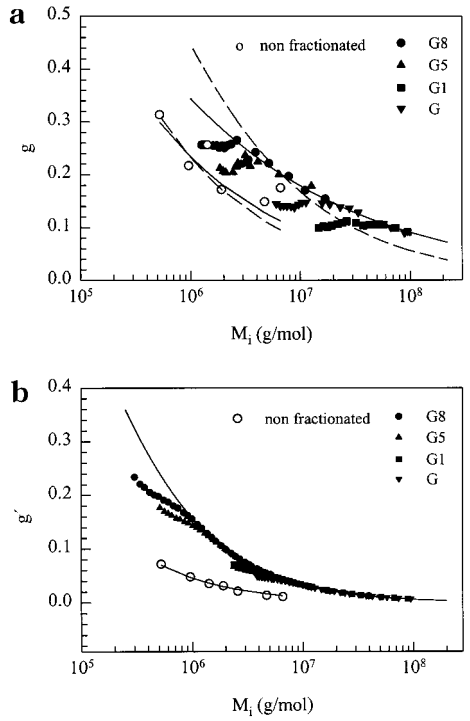

Figure 14. Molar mass dependence of g and g' shrinking factors, derived from the fractionated samples (filled symbols). This is compared with the results for the nonfractionated samples. The dashed line in Figure 14a corresponds to the Zimm−Stockmayer theory. A fit was possible only by modification of this formula due to eq 14. A fit for the nonfractionated samples was possible with the theory of Burchard,[29a,b] where again the full line corresponds to modified eq 16. The full line in Figure 14b corresponds to the modified Zimm−Stockmayer theory, using the relationship of $g' = g^{2.46}$. A similar fit was possible with the unfractionated sample, using here the experimental value of 2.11. The fit parameter is a proportionality factor between the molar mass and the number of branching points. Very different values were obtained, which indicates a more complex branching process then expected from the idealized statistical model of hyperbranching.

Most interesting is, of course, whether a branching density could now be derived from the molar mass dependencies of g and g' for the fractions. (Note: Two relationships were used to describe the curves in Figure 11 for the nonfractionated samples and in Figure 14a,b for the fractions from SEC slices).

For the interpretation of the fractions from the SEC slices, we used the Zimm−Stockmayer relationship as was already mentioned. A modification with an exponent of 0.3 instead of 0.5 was necessary to receive a good

description. The exponent b in the relationship between g' and g is now $b = 2.45$ (Figure 12).

The fit of the g values by the modified Zimm−Stockmayer relationship gave a value of $\lambda = 2.08 \times 10^{-4}$ mol/g, or $M_0 = 4826$, which would correspond to a segment length of 29 α(1,4)-linked glucose units that connects two branching points. Expressed in notations of the hyperbranched model, the branching probability corresponds to $p(1 - p) = 0.035$, which is smaller than the $p(1 - p) = 0.08$ that was obtained from the chemical analysis of permethylated and fully degraded glycogens. This discrepancy probably results from the wrong model, i.e., from the random three-functional polycondensation, as was already mentioned when discussing the properties of nonfractionated samples. On the other hand, the applied simplified hyperbranched model has to be replaced by a complex model, because of the observed heterogeneity in structure. In addition, Gaussian statistics can no longer be expected.

6. Conclusion

On the basis of nonfractionated glycogen samples, most experiments agree in behavior with that prediction for hyperbranched macromolecules. Quantitatively, however, a much lower branching density is found from the polydispersity than that derived from the analysis of monomer units of permethylated samples, when a complete degradation was applied. Two main reasons can be shown to be responsible for several uncommon values of the structural parameters. However, a reasonable agreement with theory was found from the so-called shrinking parameters when a modified equation for hyperbranching is applied. The two mentioned reasons are as follows:

(1) According to SEC, all samples appear to be composed of two components. These two components differ in their physical−chemical behavior.

(2) Current theories are based on idealized models that cannot take account of heterogeneities in branching. Furthermore, the effect of excluded volume cannot at present be taken into account. The apparently existing homogeneous segment density distribution with a well-defined periphery for the high M_w compound may probably be caused by volume exclusion.

The heterogeneity in the branched structure is already known from α-amylase degradation experiments of Schramm,[32] who received after exhausting degradation an α-limiting dextrin of rather high molar mass. In a corresponding experiment in the Freiburg laboratory,[33] which was carried out 20 years ago, a molar mass of $M_w = 35\,000$ was found for the α-limiting dextrin. Evidently, the biosynthesis of glycogen proceeds not statistically but follows a more complex route. Further experiments are in progress. Among others, the α-amylase degradation will be repeated, and the α-limiting dextrin will exhaustively be analyzed with the more powerful techniques of modern analysis.

Acknowledgment. We acknowledge the generous support of the Deutsche Forschungsgemeinschaft on the basis of a memorandum between the Romanian Academy and Deutsche Forschungsgemeinschaft. C.E.I. affectionately thanks the DFG for the opportunity of a 3 month grant for work at the Freiburg Laboratory.

Appendix 1

Alternative Definition of Degree of Branching. Modern NMR analysis often allows assignment of special peaks to monomer units in which (i) both B-functionalities have a reacted dendric unit (D), (ii) only one has a reacted linear unit (L), and (iii) terminal units (T) in which neither of the two B-groups have reacted. Chemists are presently very interested in dendric structures, which results in a different definition of a branching density:

$$\mathrm{DB} = \frac{D}{D_{\max}} = \frac{2D}{2D + L} \tag{A1}$$

where D is the number of experimentally found dendric units and $D_{\max}$ is the maximum possible dendric structures that can be expressed in terms of D and L units. For details, Schramm[32] may be consulted. Thus, a perfect dendrimer has a DB = 1 (100% branching). However, the ratio of branching units to all built in monomer units gives only $B/N = 0.5$ (50% branching points), because the terminal groups equal the branching points in the dendrimer. The branching probability is smaller by approximately a factor of 2 than the degree of branching used by chemists. The two definitions become identical when all outer chains are cleaved near the outward branching units. Such structures can be realized with amylopectin and glycogen by the action of β-amylase, an exoenzyme, which successively cleaves maltose from linear chains, until only stubs of 1−2 monomers remain before a branching unit. These structures are called β-limiting dextrins.

Appendix 2

Polydispersity and Structural Parameters for Hyperbranched Samples. The introduction of probabilities of reaction assigned to the individual functional groups was first made by Flory. It has the advantage that with probabilities (= extent of reaction) size distribution function and the corresponding molar mass averages can be derived. For the $A\langle^{B_1}_{B_2}$ monomers, this was done by Erlander and French and gave the following:

$$M_n = M_0/(1 - \alpha) \tag{A2}$$

$$M_w = M_0 \frac{1 - \alpha^2 2p(1 - p)}{(1 - \alpha)^2} \cong M_0 \frac{1 - 2p(1 - p)}{(1 - \alpha)^2} \tag{A3}$$

resulting in the following approximation for the polydispersity ratio

$$\frac{M_w}{M_n} \cong 1 + [2p(1 - p)]^{1/2}(\mathrm{DP}_w^{1/2} - 1) \tag{A4}$$

In 1972, the theory was further extended to the derivation of the angular dependence of scattered light intensities, the radius of gyration R_g, and the hydrodynamic radius R_h.[3,10,29] Here, we quote only the results for the ρ-parameter and the shrinking factor:

$$\rho \equiv \frac{R_g}{R_h} = \left[\frac{3(1 + 2B_n)}{4(1 + B_n)}\right]^{1/2}\left(\frac{2 + B_n}{1 + B_n}\right) \tag{A5}$$

$$g = \frac{R_{g\,b}^2}{R_{g\,\mathrm{lin}}^2} = \frac{6[1 + 2B_w]^{1/2}}{[1 + (1 + 2B_w)^{1/2}]^2} \tag{A6}$$

where $B_n = p(1 - p)\mathrm{DP}_n$ and $B_w = B_n(M_w/M_n)$.

References and Notes

(1) Burchard, W.; Keppler, D.; Decker, K. *Makromol. Chem.* **1968**, *115*, 350.
(2) Orrel, S. A.; Bueding, E. *J. Biol. Chem.* **1964**, *239*, 4021.
(3) Burchard, W. *Macromolecules* **1977**, *10*, 919.
(4) Rosati, G. *J. Ultrastruct. Res.* **1967**, 444.
(5) (a) Drochmans, P. *Biochem. Soc. Sympos.* **1963**, *23*, 127. (b) Drochmans, P.; Danton, E. *Control of Glycogen Metabolism*; Academic Press: London, 1968; p 187.
(6) Mischnick, P. University of Braunschweig, personal communication.
(7) Aberle, T.; Burchard, W.; Vorwerg, W.; Radosta, S. *Starch/Stärke* **1994**, *46*, 329.
(8) Flory, P. J. *Principles in Polymer Chemistry*; Cornell University Press: Ithaca, N. Y. 1953.
(9) Erlander, S.; French, D. *J. Polym. Sci.* **1956**, *20*, 7.
(10) Burchard, W. *Macromolecules* **1972**, *5*, 604.
(11) De Gennes, P. G. *Scaling Concepts in Polymer Physics*; Cornell University Press: Ithaca, N. Y., 1979.
(12) Galinsky, G.; Burchard, W. *Macromolecules* **1996**, *29*, 1498.
(13) Daoud, M.; Martin, J. E. In *The Fractal Approach to Heterogeneous Chemistry*; Avenir, D., Ed.; Wiley: New York, 1992.
(14) Aberle, T.; Burchard, W. *Starch/Stärke* **1997**, *49*, 215.
(15) Aberle, T.; Burchard, W. *Comput. Theor. Polym. Sci* **1997**, *7*, 215.
(16) Fox, J. D.; Robyt, J. F. *Carbohydr. Res.* **1992**, *227*, 163.
(17) Nelson, N. *J. Biol. Chem.* **1944**, *153*, 375.
(18) Burchard, W. *Adv. Polym. Sci.* **1999**, *143*, 113.
(19) Bareiss, R. E. In *Polymer Handbook*, 2nd ed.; Brandrup, J., Immergut, E. H., Eds.; Wiley: New York, 1975; IV 119.
(20) Stauffer, D. *Introduction to Percolation Theory;* Taylor & Francis: Philadelphia, 1985.
(21) Burchard, W.; Schmidt, M.; Stockmayer, W. H. *Macromolecules* **1980**, *13*, 1265.
(22) Galinsky, G.; Burchard, W. *Macromolecules* **1995**, *28*, 2363.
(23) (a) Kirkwood, J. G.; Riseman, J. *J. Chem. Phys.* **1948**, *16*, 565. (b) Eirich, F. R. *Rheology: Theory and Applications*; Academic Press: London, 1956.
(24) Yamakawa, H. *Modern Theory of Polymer Solutions*, Harper & Row: New York, 1972.
(25) Rey, A.; Freire, J. J.; Garcia de la Torre, J. *Macromolecules* **1987**, *20*, 342.
(26) Zimm, B. H.; Stockmayer, W. H. *J. Chem. Phys.* **1949**, *17*, 1301.
(27) Stockmayer, W. H.; Fixman, M. *Ann. N. Y. Acad. Sci.* **1953**, *57*, 334.
(28) Weismüller, M.; Burchard, W. *Acta Polym.* **1997**, *48*, 571.
(29) (a) Burchard, W. *Adv. Polym. Sci.* **1983**, *48*, 1. (b.) Galinsky, G.; Burchard, W. *Macromolecules* **1997**, *30*, 4445.
(30) Kurata, M.; Abe, M.; Imwama, M.; Matsushima, M. *Polym. J.* **1972**, *3*, 729.
(31) Zimm, B. H.; Kilb, R. W. *J. Polym. Sci.* **1959**, *37*, 19.
(32) Schramm, M. In *Control of Glycogen Metabolism*; Whelan, W. J, Ed.; Academic Press: London, New York, 1968; p 179.
(33) Reiner, A. Ph.D. Thesis, University of Freiburg, 1981.
(34) Hölter, D.; Burgath, A.; Frey, H. *Acta Polym.* **1997**, *48*, 298.
(35) (a) Burchard, W. *Makromol. Chem.* **1963**, *59*, 16; (b) **1968**, *64*, 110.
(36) Stivala, S. S.; Zweig, J. J.; Ehrlich, J. In *Solution Properies of Polysaccharides*; Brant, A. A., Ed.; ACS Symposium Series 150; American Chemical Society: Washington, DC, 1981; p 101.

MA990600M